

Progradational sand-mud deltas in lakes and reservoirs. Part 1. Theory and numerical modeling

Formation des deltas de sable et de boue dans les lacs et les réservoirs. 1^{ière} Partie. Théorie et modélisation numérique

SVETLANA KOSTIC and GARY PARKER, *St. Anthony Falls Hydraulic Laboratory, University of Minnesota, Minneapolis, MN, 55414, USA*

ABSTRACT

Deltas are cone-shaped deposits formed at the confluence of rivers with standing bodies of water. One of the most common stream morphologies associated with deltas is that of the sand-bed stream. Such streams usually carry significantly more mud as wash load than they do sand as bed material load. Deltas typically form so that the sand deposits fluvially in the river channel and avalanches into deeper water to create a prograding delta face. The remaining muddy river inflow often plunges over the steep delta face and continues flowing downslope as a bottom turbidity current. The mud carried into deep water by the underflow settles out on the bed of the lake or reservoir. A variety of numerical models dealing separately with either fluvial deposition or depositional turbidity currents have been proposed to date. The work reported here pertains to an integral, physically-based, moving boundary model of deltaic sedimentation in lakes and reservoirs that captures the co-evolution of the river-delta morphology and the associated deposits. The formulation unites fluvial and turbidity current morphodynamics in a single numerical model. The model is tested against the results of the two experiments described in a companion paper.

RÉSUMÉ

Les deltas sont les dépôts en forme de cône formés au confluent des fleuves avec des eaux stagnantes. Une des morphologies de courant les plus communes associées aux deltas est celle du courant de lit de sable. De tels courants portent habituellement sensiblement plus de boue comme charge de lessivage que de sable en tant que matériau de lit. Typiquement, les deltas se forment de la façon suivante: le sable se dépose dans le chenal de la rivière et se déverse en avalanches vers l'eau plus profonde en créant un front progressif de delta. L'apport boueux restant plonge généralement au-dessus de la pente raide du delta et continue sa descente tel un courant de turbidité. La boue transportée par ce courant de fond vers les eaux plus profondes, se dépose au fond du lac ou du réservoir. On a proposé jusqu'ici une variété de modèles numériques traitant séparément le dépôt fluvial ou les courants de dépôts de turbidité. Le travail rapporté ici concerne un modèle intégral, basé sur la physique, avec une frontière mobile de la sédimentation en delta dans les lacs et réservoirs qui sont le siège de l'évolution de la morphologie de delta de fleuve et des dépôts associés. La formulation unit la morphodynamique du courant fluvial et de la turbidité dans un modèle numérique simple. Ce modèle est testé en le confrontant aux résultats de deux expériences décrites dans un article associé.

Keywords: Deltaic sedimentation; turbidity current; physically-based model; moving boundaries; time stretching; stratified ambient; bed evolution.

1 Introduction

Deltas commonly display three distinct zones; (a) a low-slope topset deposit that forms as the coarse sediment load deposits on the river bed, (b) a high-slope foreset deposit (delta face) that forms as the coarse sediment load avalanches down the delta face into deeper water and (c) a low-slope bottomset deposit that forms as the fines settle out on the bed of the lake or reservoir. This structure is illustrated in Figure 1a (e.g. Vanoni, 1975).

Rivers generally carry a broad range of sediment sizes. Here the problem is abstracted to sand-bed rivers that predominantly transport two grain sizes, sand and mud. Such rivers typically

have beds that are composed almost exclusively of sand, i.e. material between 62 and 2000 μm . In terms of an annual average, however, the great majority (90% or more) of the sediment load carried by these streams is often in the range of silt and clay, here grouped together as "mud."

A case in point is the Nemadji River, which originates in Minnesota and flows into Lake Superior at Superior Harbor, Wisconsin (Figure 2). The mean annual loading of this stream at Superior Harbor has been estimated to be 131,000 tons/year, 11 percent of which is sand, the remaining 89 percent being mud (Cooper and Lensch, 1998). The sand deposits out to form a delta in Superior Harbor. This delta must be removed by dredging in order to maintain navigation in the harbor. Most of the mud,

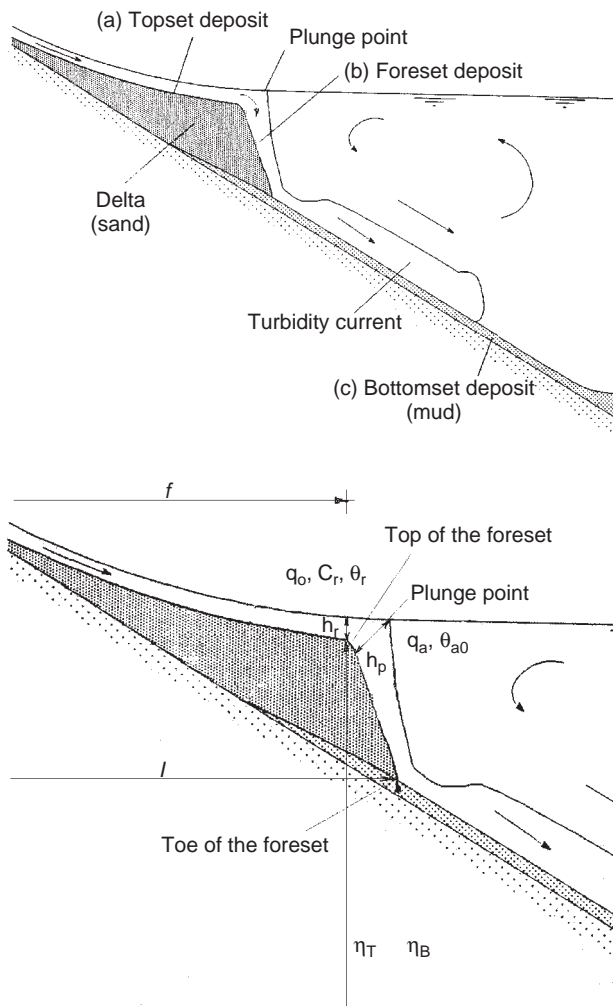


Figure 1 (a) Definition diagram showing the structure of a deltaic deposit in a lake or reservoir. (b) Definition diagram of relevant parameters for plunging and shock condition at foreset.



Figure 2 The Nemadji River as it flows into Lake Superior at Superior Harbor, Wisconsin. Plunging of the current can be seen in the upper right-hand corner of the image.

however, remains in suspension and is transported out into the deep water of the lake.

The mud carried by a sand-bed stream typically forms only a negligible fraction of the bed material because its deposition on the river bed is inhibited by the relatively high ratio of boundary shear velocity to particle fall velocity. For this

reason it is often referred to as wash load. In the deltas of sand-bed streams, therefore, the topset and foreset deposits are built mostly out of sand, while the bottomset deposit consists mostly of mud. The mud may be deposited by one of three mechanisms. The first of these consists of surface plumes and the second consists of interflows. Both of these form when the sediment-laden river inflow has a density that is less than the highest density of water in the lake or reservoir. The third mechanism is a muddy bottom turbidity current which forms when the sediment-laden river inflow is sufficiently heavy to plunge. Since the delta face is generally one or two orders of magnitude steeper than the topset face, water depth in the lake or reservoir increases relatively rapidly downslope. As a result, plunging often occurs only a short distance beyond the top of the foreset deposit, as shown in Figures 1a and 1b. Plunging may be inhibited if temperature stratification renders the density of the standing fresh water higher than that of the river water. The wash load of many rivers is high enough to ensure plunging during floods, when river sediment delivery is the highest. Streams in Minnesota, for example, transport almost 25% of their annual suspended sediment load during the April snowmelt event (U.S. Geological Survey, 1986). It is therefore likely that in many deltas bottomset deposits are mostly the result of the deposition from underflows rather than hemipelagic rain from surface plumes or interflows.

Sustained plunging turbidity currents have been observed in many reservoirs and lakes (e.g. Normark and Dickson, 1976; Lambert, 1982; Fan, 1986; Chikita, 1989). Some of the oldest measurements were taken on Lake Mead, a reservoir on the Colorado River (Grover and Howard, 1937). Figure 3a illustrates the pattern of deltaic deposition in the reservoir between 1935 and 1948. Of particular interest is the interface between the sandy foreset and muddy bottomset deposit, which is seen in Figure 3b to migrate both in the streamwise and vertical direction over time. The loss of available storage and other repercussions of reservoir sedimentation have been underlined by various authors (e.g. Mahmood, 1987; Sloff, 1997). Moreover, a variety of numerical models for the deposition of bed-material load in reservoirs have been proposed (e.g. Hotchkiss and Parker, 1991). Similar models of turbidity currents in reservoirs have also been developed (e.g. Sloff, 1997).

The work presented here is a full numerical model of deltaic sedimentation in lakes and reservoirs. The model consists of two linked submodels: (1) a turbidity current model that describes the evolution of the bottomset deposits, and (2) a fluvial delta model that describes the evolution of the prograding topset and foreset deposits. The model tracks three moving boundaries. The first two boundaries define the position of the top and bottom of the delta face, respectively, and move at geomorphic or slow time scale. The third boundary follows the head of the turbidity current, and moves at hydraulic or swift time scale. The morphology of the resulting deposits, and the evolution of the sand-mud interface in particular is strongly affected by the interplay between fluvial and turbidity current deposition. The results of a verification of the model outlined here are reported in a companion paper, Kostic and Parker (2003).

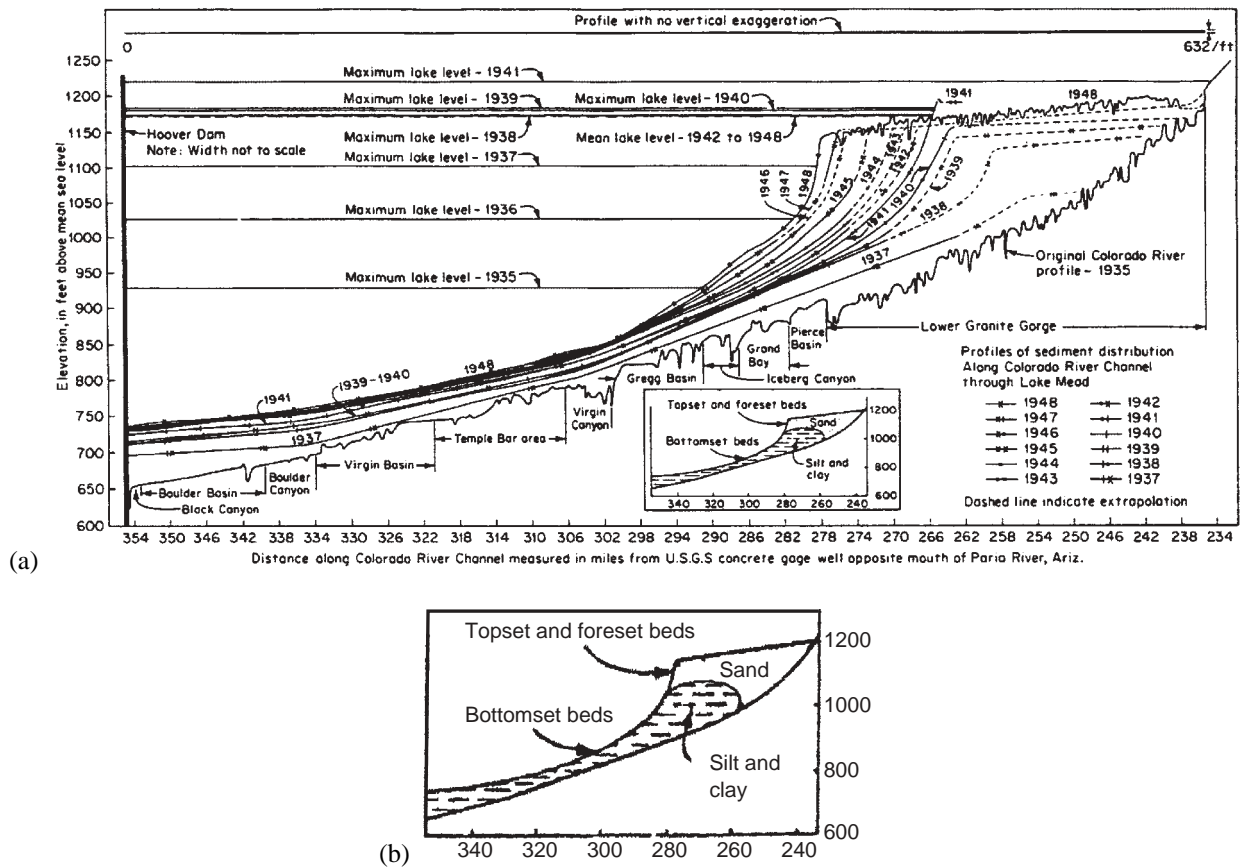


Figure 3 (a) Deposition pattern along the Colorado River through Lake Mead, 1935–1948. From Graf (1971), based on an original in Grover and Howard (1937). (b) Expansion of an inset in Figure 3a illustrating the time evolution of the boundary between the sandy topset and foreset deposits and the muddy bottomset deposits in Lake Mead.

2 Model formulation

The following assumptions and approximations are introduced in order to simplify the problem:

1. The delta is simplified to a 1-D configuration. That is, the delta and its associated deposits are allowed to prograde in the longitudinal direction but not allowed to flare out in the transverse direction. This approach allows for a relatively simple experimental test of the model, as described in the companion paper. The model can be easily generalized to a quasi 2-D laterally expanding model of river deltas in lakes and reservoirs.

2. The sediment consists of sand and mud, represented only by the median diameters D_S and D_M respectively. The river flow carries the sand as bed-material load, which moves both as bedload and suspended load, and the mud as wash load, which is entirely in suspension. The sand is too coarse to be carried by the muddy bottom turbidity current, while the mud is too fine to deposit on the river bed or delta face. This gross simplification is nevertheless reasonable as a first-order approximation of many deltas, as illustrated in Figure 3. Implicit in this abstraction is the assumption that the cutoff between sand and silt, i.e. $62.5 \mu\text{m}$, is also the cutoff between bed-material load and wash load. This is not necessarily the case (Paola and Parker, 2000), but is nevertheless a reasonable first approximation for the present analysis.

3. The river originates at a point $x = 0$ where the water discharge per unit width q_w and the volume discharge per unit width

of sand q_{S0} and mud q_{M0} are prescribed as functions of time. Tributaries are not included in the model, and thus a spatially constant water discharge is maintained down the river.

4. The foreset is deposited at a spatially constant avalanche slope S_a . This slope may not exceed the angle of repose of the sand, but in many cases can be well below the angle of repose due to the destabilizing effect of a turbidity current passing over it, as described in Kostic *et al.* (2002).

5. Deposition of mud by fallout from surface plumes and interflows is neglected. The model can be amended to include this effect at a later date.

6. The hydrodynamic part of the turbidity current model is based on a standard layer-integrated slender flow formulation, descended from the work of Ellison and Turner (1959) on simple density currents, but in which time variation has been added and the top-hat assumption has been employed to define the shape constants (Parker *et al.*, 1986). The hydrodynamic unit, however, has been modified to include density stratification due to temperature as well as sediment. It also accounts for the possibility of ambient stratification in the lake or reservoir (Baines, 1999).

7. The depth of the lake or reservoir is considerably larger than the depth of turbidity current. Thus, flow in the ambient upper layer can be approximated as having no dynamic effect on the underflow, and a single-layer turbidity current model can be adopted. In addition, the elevation of the water surface of the lake is held constant.

8. The turbidity current is sufficiently dilute to allow the use of the Boussinesq approximation in the equations of motion, and to neglect the effect of hindering settling of mud.

9. The turbidity current is too weak to entrain mud from the bottom of the lake or reservoir. Thus, only deposition is considered. The model can be easily modified to include entrainment once the entrainment relation is known (e.g. Parker *et al.*, 1986).

10. The net effect of the suspended sediment and temperature differences renders the river inflow heavier than the ambient water. A simple linear relation between density and temperature is used here. This assumption can easily be relaxed, however, to allow for nonlinear effects that are particularly important near 4°C. The ambient water is sediment-free and stratified. The upward normal scale of density variation in stratified flow is large compared to underflow thickness, so the effect of the ambient stratification is expressed as $\rho_a = \rho_a(x)$, where ρ_a is the extrapolation of the ambient density to the bed of the lake or reservoir and x is an arc length streamwise coordinate taken along the bed.

11. The river flow is modeled as steady, whereas the full time evolution of the turbidity current is analyzed. This is for the following reason. The variation of discharge in many low-slope rivers is sufficiently gradual so as to allow the assumption of steady flow in each step of a hydrograph. The turbidity current, however, may be turned on or off suddenly depending on whether or not the criterion for plunging of the river flow is met.

3 Continuity and shock conditions at the foreset

The present model consists of a fluvial submodel and a turbidity current submodel, which are linked to each other by the avalanching foreset of Figure 1a,b. Where x denotes a streamwise coordinate and η denotes bed elevation, the elevation profile of the foreset is given by the simple relation

$$\eta = \eta_T - S_a(x - f) \quad (1)$$

where f is the distance to the topset–foreset break and η_T denotes the bed elevation there. One condition linking the two submodels is the imposition of bed elevation continuity at the foreset–bottomset break. That is,

$$\eta_B = \eta_T - S_a(l - f) \quad (2)$$

where l denotes the distance to the foreset–bottomset break and η_B is the elevation there.

A second condition linking the two models is a shock condition that can be obtained by integrating the Exner equation of sediment continuity over the foreset. This equation takes the form

$$(1 - \lambda_S) \frac{\partial \eta}{\partial t} = - \frac{\partial q_S}{\partial x} \quad (3)$$

where λ_S denotes the porosity of the sand deposit of the foreset, t is time and q_S is the volume sand transport rate per unit width due to avalanching. In the Appendix Eq. (3) is integrated across the foreset, i.e. from $x = f$ to $x = l$ under the constraint of (2) and the condition that the sand transport rate q_S vanishes at the

toe of the foreset. After some manipulation and approximation the following result is obtained;

$$q_S|_{x=f} = (1 - \lambda_S) \dot{f} (\eta_T - \eta_B) \quad (4)$$

Simply stated, this shock condition progrades the foreset by placing all of the sand delivered from the fluvial topset to the foreset so as to maintain constant foreset slope S_a .

4 Turbidity current submodel

4.1 Governing equations

The spatial development of an unsteady, one-dimensional, depositional turbidity current driven by excess density due to suspended sediment, and driven or hindered by temperature difference with the near-bottom ambient water can be described by the following set of layer-averaged equations (Parker *et al.*, 1986; Baines, 1999):

$$\frac{\partial h}{\partial t} + \frac{\partial U h}{\partial x} = e_w U \quad (5)$$

$$\frac{\partial U h}{\partial t} + \frac{\partial U^2 h}{\partial x} = - \frac{1}{2} g \frac{\partial (RC - \beta \theta_d) h^2}{\partial x} - g h (RC - \beta \theta_d) \frac{\partial \eta}{\partial t} - u_*^2 \quad (6)$$

$$\frac{\partial C h}{\partial t} + \frac{\partial C U h}{\partial x} = - \Delta \quad (7)$$

$$\frac{\partial \theta_d h}{\partial t} + \frac{\partial \theta_d U h}{\partial x} = - U h \frac{\partial \theta_a}{\partial x} \quad (8)$$

where t is time, x is the downslope distance along the bottom of the lake or reservoir, e_w is the water entrainment coefficient, β is a local thermal expansion coefficient obtained from a linear expansion of the relation between water density and temperature, η is the elevation of the bottomset deposit, u_* is the shear velocity, Δ is the volume deposition rate per unit area of the mud on the bed, θ_a is the ambient temperature near the bed and R is submerged specific gravity of mud, here assumed to be equal to 1.65. The dependent variables are the current depth h , the depth-averaged velocity U , the depth-averaged volumetric concentration of suspended sediment C and the depth-averaged temperature deviation θ_d , here defined to be the difference between the layer-averaged current temperature and the ambient temperature near the bed.

The hydrodynamic part of the model thus consists of the conservation of fluid mass, i.e. Eq. (5) and the conservation of downslope momentum, i.e. Eq. (6). The term $e_w U$ in the continuity equation describes the rate of clear water entrainment from the ambient water above into the underflow. In the momentum equation the first term on the right-hand side represents the effect of the downslope pressure gradient caused by the suspended sediment and the temperature difference between current and ambient water, the second term is the downslope force per unit bed area of the gravity on the sediment-water mixture and the third term represents the flow resistance due to bottom friction. The transport part of the model includes the conservation of suspended sediment mass, i.e. Eq. (7), and the conservation of heat, i.e. Eq. (8).

The elevation of the bottomset deposit is gradually altered as a consequence of mud deposition from the current, and thus the sediment-laden flow and the bed of the lake or reservoir constitute a physically coupled system. That is, deposition from the flow changes the bed morphology, and the resulting change in the bed slope changes the flow. The elevation of bed is computed from the Exner equation; where λ denotes the porosity of the bottomset deposit,

$$(1 - \lambda) \frac{\partial \eta}{\partial t} = \Delta \quad (9)$$

4.2 Closure relations

In order to close the set Eqs. (5)–(9) internal relations for the water entrainment coefficient e_w , shear velocity u_* and deposition rate Δ must be specified.

Parker *et al.* (1986) present the following relation describing water entrainment coefficient for dense underflows:

$$e_w = \frac{0.00153}{0.0204 + Ri} \quad (10)$$

where Ri is the bulk Richardson number, defined as

$$Ri = \frac{gh(RC - \beta\theta_d)}{U^2} \quad (11)$$

In the momentum equation shear velocity u_* is related to the mean velocity U by means of a bottom friction coefficient c_D :

$$c_D = \frac{u_*^2}{U^2} \quad (12)$$

In general, the coefficient of bed drag c_D is a function of boundary-layer parameters. According to Parker *et al.* (1987), the value of c_D is between 10^{-3} and 10^{-1} for one-dimensional turbidity currents with Reynolds number in the range $[4 \cdot 10^2, 2 \cdot 10^6]$. Herein, c_D is taken to be constant in the downstream direction for simplicity.

The deposition rate Δ is specified in terms of the mud fall velocity v_M and the near-bed volumetric sediment concentration c_b , which is related to the layer-averaged concentration C by a multiplicative constant r_0 . Thus,

$$\Delta = v_M r_0 C \quad (13)$$

In the experiments carried out by Parker *et al.* (1987) the value of r_0 was found to be nearly constant and equal to 2.0 for turbid underflows. This value is adopted here in the absence of other information. The mud fall velocity v_M is calculated from the relation of Dietrich (1982).

4.3 Non-dimensionalization

The above governing equations are placed in dimensionless form, which allows interpretation of the numerical results at arbitrary scale.

$$\begin{aligned} \hat{x} &= \frac{x}{h_0}, & \hat{h} &= \frac{h}{h_0}, & \hat{\eta} &= \frac{\eta}{h_0}, & \hat{\theta}_d &= \frac{\theta_d}{\theta_0}, & \hat{\theta}_a &= \frac{\theta_a}{\theta_0}, \\ \hat{U} &= \frac{U}{U_0}, & \hat{v}_m &= \frac{v_m}{U_0}, & \hat{C} &= \frac{C}{C_0}, & \hat{t} &= \frac{t}{h_0/U_0} \end{aligned} \quad (14a-i)$$

Here U_0 , h_0 , C_0 and θ_0 denote the values of the velocity U , depth h , volumetric concentration C and deviation θ_d from the ambient bottom temperature immediately after the river inflow plunges to form a turbidity current.

The governing dimensionless parameters for the problem at hand are as follows.

The Richardson number Ri_0 immediately after plunge point expresses the ratio of the buoyancy to inertial force, and is given by

$$Ri_0 = \frac{gh_0(RC_0 - \beta\theta_0)}{U_0^2} \quad (15)$$

The buoyancy ratio φ_{S0} immediately after plunge point represents the fraction of the buoyancy force that derives from the presence of suspended sediment (as opposed to temperature difference), and is given by

$$\varphi_{S0} = \frac{RC_0}{RC_0 - \beta\theta_0} \quad (16)$$

The particle Reynolds number R_p is given by

$$R_p = \frac{(RgD_M)^{0.5} D_M}{\nu} \quad (17)$$

where D_M is the median grain size of mud and ν is the kinematic viscosity of water, here taken to be equal to the value 10^{-6} m²/s.

The remaining dimensionless governing parameters are: bottomset friction factor c_D , volume suspended sediment concentration C_0 just beyond the plunge point, submerged specific gravity of mud R , porosity of the mud deposit λ , here taken to be constant, and initial slope S_0 of the bottomset deposit, here assumed to be constant for simplicity.

4.4 Plunging

A sufficiently turbid river entering a lake or a reservoir pushes the ambient water outward until a threshold condition is reached. At this point a “plunge line” forms; the current sinks and continues flowing downslope as a bottom turbidity current. In general, the flow width increases with the distance downstream from the river mouth, and thus the plunge phenomenon is three dimensional. However, if the change in flow width is not too large plunging can be considered as two-dimensional, with the plunge line devolving to a plunge point.

Numerous relations for prediction of the plunge depth h_p in a channel of constant width can be found in the literature (e.g. Singh and Shah, 1971; Savage and Brimberg, 1975; Jain, 1981; Akiyama and Stefan, 1984). These relations are typically expressed in terms of a densimetric Froude number Fr_p associated with plunging, here defined as

$$Fr_p = \left(\frac{q_o^2}{\varepsilon g h^3} \right)^{1/2} \quad (18)$$

where q_o is the river water discharge per unit width just before plunging and ε is the inflow density, given by

$$\varepsilon = RC_r - \beta(\theta_r - \theta_{a0}) \quad (19)$$

where C_r is the volumetric concentration of wash load in the river just before plunging, θ_r is the river temperature just before

plunging and θ_{a0} is the ambient temperature at the river mouth (Figure 1b). The densimetric Froude number at the plunge point has commonly been determined empirically. It has, however, been found to depend on the foreset slope and the total friction factor accounting for both bed and interfacial friction in the plunge region. Akiyama and Stefan (1987) provide a very comprehensive summary of values of Fr_p from the literature. For channels of constant width the range $0.1 \leq Fr_p \leq 0.7$ was observed for slopes in the range $10^{-3} \leq S \leq 10^{-1}$, with a typical value of $Fr_p = 0.56$. Once Fr_p is set the value of h_p can be computed from (18).

Akiyama and Stefan (1984) employed dimensionless analysis to illustrate that channel slope is one of the essential independent parameters governing the plunging flow. They used conservation of mass, volume and momentum to determine the plunge depth and the underflow properties immediately after the plunge point in channels with both mild and steep slopes. The plunging flow on a steep slope changes from Froude-subcritical ($Ri > 1$) upstream of the plunge point to Froude-supercritical ($Ri < 1$) downstream of that point. The plunge depth h_p in a steep channel is defined as follows:

$$h_p = \frac{h_r Ri_r^{-1/3}}{2(S_1)^{1/3}} \times \left[\frac{2 + \gamma}{2} + S_1 + \sqrt{\left(\frac{2 + \gamma}{2} + S_1\right)^2 - \frac{4S_1}{1 + \gamma}} \right] \quad (20)$$

where Ri_r is the river Richardson number, here defined as

$$Ri_r = \frac{\epsilon g h_r^3}{q_o^2} \quad (21)$$

where h_r denotes the river depth at the top of the foreset, i.e. somewhat upstream of the plunge point. γ is an initial mixing coefficient associated with plunging and S_1 is a shape factor, accounting for nonuniform density distribution over the depth. According to experiments conducted by Garcia and Parker (1993), $S_1 \cong 1$ for turbidity currents. The mixing coefficient is defined as a ratio of ambient to river flowrate per unit width, i.e. $\gamma = q_a/q_o$, and is calculated from the relation developed by Farrell and Stefan (1988) that is multiplied by the correction factor 0.1/0.23. The correction is introduced because the authors reported this amount of disagreement between predicted and measured mixing coefficients.

The above plunging formulation is incorporated in the numerical model of turbidity currents as particularly suitable for the case of plunging over a steep delta face with a foreset slope that is at least 1° .

4.5 Numerical technique

Two aspects of the problem make the turbidity current modeling intriguing from a numerical point of view. First, the inflow and outflow boundaries of the current are moving boundaries, and their positions must be determined as functions of time along with the flow field. The inflow boundary moves downstream slowly as the river delta progrades into the lake or reservoir, and the

outflow boundary moves rapidly with the head of the turbidity current. Second, the governing equations are of hyperbolic type, admitting shocks and discontinuities, and the numerical method selected to analyze the problem must be capable of capturing the underlying physics of such phenomena.

4.5.1 Front-fixing method

Since both the inflow and outflow boundaries of the current are moving, an alternative to their tracking is to fix them by a suitable choice of new coordinate system. Here a Landau transformation (Crank, 1984) is used to map the spatial domain into to the finite interval $x^* \in [0, 1]$, with the position of the foreset toe at the fixed point $x^* = 0$ and the position of the current front head at $x^* = 1$:

$$\begin{cases} x^* = \frac{x - l(t)}{s(t) - l(t)}, & 0 \leq x^* \leq 1 \\ \tau = t \end{cases} \quad (22a,b)$$

In the above relation, l denotes the dimensionless position of the foreset toe. The parameter s has one of two definitions depending upon how the model is implemented. The base definition is the position of the front of the turbidity current, in which case no outflow is allowed beyond $x^* = s$. In some implementations, however, it is useful to fix s in space, in which case outflow is allowed beyond $x^* = s$. When the latter definition is used in the present work, the value of s is determined in terms of a specified target concentration \hat{C}_t . The space and time derivatives are given by

$$\begin{aligned} \frac{\partial}{\partial t} &= \frac{\partial}{\partial \tau} + \left(\frac{x^* - 1}{s - l} \dot{l} - \frac{x^*}{s - l} \dot{s} \right) \frac{\partial}{\partial x^*} \\ \frac{\partial}{\partial x} &= \frac{1}{s - l} \frac{\partial}{\partial x^*} \end{aligned} \quad (23a,b)$$

where $\dot{l} = dl/dt$ and $\dot{s} = ds/dt$ are the dimensionless velocities of the toe of the foreset and the current head, respectively.

Let the conservative dimensionless variables \hat{q} , $\hat{\phi}$ and $\hat{\psi}$ be defined as follows:

$$\hat{q} = \hat{U} \hat{h} \quad \hat{\phi} = \hat{C} \hat{h} \quad \hat{\psi} = \hat{\theta}_d \hat{h} \quad (24a,b,c)$$

After applying the transformations of Eqs. (23a,b) and reducing with (24a,b,c), Eqs. (5)–(9) can be rewritten in the following conservative forms:

$$\begin{aligned} \frac{\partial h}{\partial \tau} &= \frac{1}{s - l} \left\{ [x^* \dot{s} - (x^* - 1) \dot{l}] \frac{\partial h}{\partial x^*} - \frac{\partial q}{\partial x^*} \right\} \\ &\quad + \frac{0.00153q/h}{0.0204 + Ri_0[\varphi_{s0}\phi + (1 - \varphi_{s0})\psi]h^2/q^2} \end{aligned} \quad (25)$$

$$\begin{aligned} \frac{\partial q}{\partial \tau} &= \frac{1}{s - l} \left\{ [x^* \dot{s} - (x^* - 1) \dot{l}] \frac{\partial q}{\partial x^*} - \frac{\partial}{\partial x^*} \left(\frac{q^2}{h} \right) \right\} \\ &\quad - \frac{Ri_0}{s - l} [\varphi_{s0}\phi + (1 - \varphi_{s0})\psi] \frac{\partial}{\partial x^*} \left(\frac{h}{2} + \eta \right) - C_D \frac{q^2}{h^2} \end{aligned} \quad (26)$$

$$\begin{aligned} \frac{\partial \phi}{\partial \tau} &= \frac{1}{s - l} \left\{ [x^* \dot{s} - (x^* - 1) \dot{l}] \frac{\partial \phi}{\partial x^*} - \frac{\partial}{\partial x^*} \left(\frac{q\phi}{h} \right) \right\} \\ &\quad - v_m r_0 \frac{\phi}{h} \end{aligned} \quad (27)$$

$$\frac{\partial \psi}{\partial \tau} = \frac{1}{s-l} \left\{ [x^* \dot{s} - (x^* - 1)\dot{l}] \frac{\partial \psi}{\partial x^*} - \frac{\partial}{\partial x^*} \left(\frac{q\psi}{h} \right) - q \frac{\partial \theta_a}{\partial x^*} \right\} \quad (28)$$

$$\frac{\partial \eta}{\partial \tau} = \frac{1}{s-l} [x^* \dot{s} - (x^* - 1)\dot{l}] \frac{\partial \eta}{\partial x^*} + \frac{v_m}{1-\lambda} r_0 C_0 \frac{\phi}{h} \quad (29)$$

In the above relations the hat “ $\hat{}$ ” has been omitted for simplicity; all parameters remain dimensionless.

4.5.2 Initial conditions

Most existing one-dimensional and two-dimensional turbidity current models, including those of Choi and Garcia (1995), Bradford (1996) and Imran *et al.* (1997) use a fixed grid. All of them must deal with the problem of a numerically “dry” bed (no turbidity current) downstream of the head of the current, where $h \rightarrow 0$. This condition is quite difficult to handle numerically (Akanbi and Katopodes, 1988). The deforming grid approach overcomes this problem in that it does not suffer from the necessity to track the transition to a “dry” bed by defining the initial values of the dependent variables in a specific manner that allows the numerical model to work. In the present analysis, at $t = 0$ the dimensionless primitive variables h , U , C and θ_d are set equal to 1.0 at all nodal points within the initially specified value of the length s from the delta toe to the front.

4.5.3 Hydrodynamic boundary conditions

For a hyperbolic system of equations, the number and location of physical boundary conditions are the number and location of characteristics that propagate into the flow domain. There are four characteristic velocities for the flow. In the transformed coordinate system they are given by:

$$c_0 = \frac{1}{s-l} [-x^* \dot{s} + (x^* - 1)\dot{l}] \quad (30)$$

$$c = \frac{1}{s-l} [U - x^* \dot{s} + (x^* - 1)\dot{l}] \quad (31)$$

$$c_{\pm} = \frac{1}{s-l} \left\{ [U - x^* \dot{s} + (x^* - 1)\dot{l}] \pm \sqrt{Ri_0 h [\varphi_{s0} C + (1 - \varphi_{s0}) \theta_d]} \right\} \quad (32)$$

Here c_0 denotes the velocity that results from the transformation of the coordinate system, c defines the rate that particles are advected in the flow and c_{\pm} correspond to the forward- and backward-propagating wave speeds for shallow-water waves. The term $\sqrt{Ri_0 h [\varphi_{s0} C + (1 - \varphi_{s0}) \theta_d]}$ is analogous to the celerity of a simple gravity wave. However, the reduction factor $\sqrt{Ri_0 [\varphi_{s0} C + (1 - \varphi_{s0}) \theta_d]} / g$ implies that turbid gravity waves, being internal waves, travel more slowly than their counterparts in shallow water. Note also that only four characteristic velocities are obtained from the set of five governing equations. This is because both the concentration of suspended sediment and the temperature difference from the ambient water contribute to the buoyancy of the flow. Thus, the transport Eqs. (27) and (28) mathematically boil down to one equation that describes the

transport of a new quantity ϑ , here defined as

$$\vartheta = \varphi_{s0} C + (1 - \varphi_{s0}) \theta_d \quad (33)$$

Hydrodynamic boundary conditions must be specified at $x^* = 0$ and $x^* = 1$. Since the turbidity currents considered here propagate downslope from the plunge point, the analysis is restricted to supercritical underflow in the Richardson sense, i.e. $Ri_0 < 1$. The model can be used in the subcritical flow regime with appropriate adjustments in the boundary conditions.

By inspection of Eqs. (30)–(32) it can be concluded that for a supercritical inflow boundary all characteristics but one propagate into the flow domain, and thus three dependent variables must be specified at $x^* = 0$, i.e. the toe of the delta face. There the parameters h , U and ϑ are set equal to 1. In doing so a very short development region between the plunge point and the toe has been omitted. In the present analysis, however, where the foreset is treated as a shock, this approximation is likely reasonable. The remaining variable η is extrapolated from the flow domain so as to describe a prograding river delta, as described below.

For supercritical outflow in the transformed coordinate system there are two characteristics propagating into the flow domain, leading to the two independent quantities that can be specified. In the model, the velocity of the last grid point is equated to the front velocity \dot{s} such that

$$U(x^* = 1, \tau) = \dot{s} = \frac{ds}{d\tau} \quad (34)$$

and the bed elevation is given by

$$\eta(x^* = 1, \tau) = \eta_0(s) \quad (35)$$

where η_0 denotes an antecedent bed elevation as yet unmodified by the turbidity current. The remaining variables are obtained from the flow domain by means of first order extrapolation, which neither destabilizes explicit schemes nor reduces the stability limits (Hirsch, 1990).

4.5.4 Numerical scheme

The modeling of highly advective transport can be difficult, even for the superficially simple case of one-dimensional constant-velocity flow. Mitchell (1984), for example, characterized advective modeling as the ultimate embarrassment of computational dynamics.

Here the difficulties associated with the present case were overcome using the QUICKEST scheme, which is an explicit finite-volume upwind algorithm designed exclusively for highly advective unsteady flows (Leonard, 1979). Since the scheme is third-order accurate, the leading truncation error is a dissipative, but not diffusive, fourth-order spatial derivative. Numerical tests for pure advection in one-dimensional flows have shown that this scheme generally gives better results than second-order central (e.g. Lax-Wendroff) and second-order upwinding schemes. However, the numerical solution obtained in the present case turns out to be highly dependent on the formulation of the physical condition (34) at the current head, resulting in unphysical overshoots and undershoots. Thus, the ULTIMATE conservative difference scheme was added to the formulation. This universal

limiter was designed by Leonard (1991), who found currently popular TVD schemes inadequate because of steepening and clipping of representative test profiles. In general, this algorithm can be applied to arbitrarily high-order transient interpolation models of the advective transport equations.

The choice of an explicit method was made because solutions of the inviscid Burgers equations computed with an implicit scheme are generally inferior to those calculated with explicit techniques, and more computational effort per integration step is required (Tannehill *et al.*, 1997). In addition, transient results are desired herein, and the larger time step permitted by implicit schemes is not of utmost importance. When discontinuities are present explicit methods are again superior. Bonnetcaze *et al.* (1993) successfully handled shocks and discontinuities in the flow with an explicit type of FDM. They noted that in explicit schemes any shock appears of its own accord from the integration, whereas implicit schemes require several algorithms for different regions of flow on either side of the shock. To know where to apply these algorithms, the shock velocity and strength must be determined as part of the problem introducing an additional complication.

The original method is significantly improved in terms of computational efficiency by the introduction of time stretching that follows grid stretching in the longitudinal direction, thus maintaining the initial Courant number. However, once the turbidity current model is linked to the fluvial model, the time stretching within the turbidity current domain becomes dependent on the significantly slower process of delta progradation. At the beginning of the calculation, the length of the turbidity current s is small, and thus the underflow Courant number imposes a limit on the time stretching in the model. The turbidity current, however, quickly begins to propagate rapidly, in which case the Courant number for the fluvial domain takes over as the limiting factor. Independently of whether the turbidity current model is used alone or linked with the fluvial model, time stretching significantly increases computational efficiency.

The present numerical model was tested against data for six experiments on weakly depositing turbidity currents conducted by Altinakar *et al.* (1990). In these experiments the inlet Reynolds number was high enough to ensure turbulent conditions at the inlet, the Richardson number was less than one and the ratio of current depth to total depth was small enough for a single-layer model to be valid. The present model was found to agree well with the data, as well as the results of the model of Choi and Garcia (1995) which employs a dissipative-Galerkin finite element method. More details about model verification can be found in Kostic and Parker (2000b).

5 Fluvial submodel

5.1 Governing equations

The flow in the fluvial zone, i.e. upstream of the top of the foreset is described by the following governing equations:

$$U_f h_f = q_w \quad (36)$$

$$\frac{\partial}{\partial \xi} \left(\frac{1}{2} U_f^2 + g h_f + g \eta_f \right) = -\frac{u_*^2}{h_f} \quad (37)$$

$$(1 - \lambda_s) \frac{\partial \eta_f}{\partial t} = -\frac{\partial q_s}{\partial \xi} \quad (38)$$

where ξ is the downslope distance along the fluvial bed, t is time, g is the acceleration of gravity, q_w denotes the water discharge per unit width, λ_s denotes the porosity of sand deposits, q_s is the volume transport rate of sand per unit width (both bedload and suspended load), and u_* is the shear velocity. The dependent variables are the depth of fluvial flow h_f , the river velocity U_f and the elevation of the river bed η_f . The hydrodynamic part of the model encompasses the quasi-steady flow approximation (e.g. De Vries, 1965), and consists of the conservation of the fluid mass, i.e. Eq. (36), and the conservation of downslope momentum as described by the St. Venant formulation for gradually varied flow, i.e. Eq. (37). The sediment part of the model is described by the Exner equation of conservation of bed sediment i.e. Eq. (38).

In order to close Eqs. (36)–(38) internal relations for the shear velocity u_* and the transport rate of sand q_s are employed. Shear velocity u_* is related to the flow velocity U_f through the bed friction factor C_f :

$$C_f = \frac{u_*^2}{U_f^2} = C_Z^{-2} \quad (39)$$

where C_Z is a dimensionless Chezy resistance coefficient. In general, C_f is a weak function of river depth, but is taken to be constant here for simplicity. The transport rate of sand q_s in Eq. (38) is computed from the Engelund-Hansen relation for total bed material load (Engelund and Hansen, 1972), and is given by

$$q_s = \sqrt{R_s g D_s} \frac{\alpha D_s}{C_f} \tau^{*2.5} \quad (40)$$

where R_s denotes submerged specific gravity of sand (again typically equal to 1.65), D_s denotes the median grain size of sand, α is a coefficient, equal to 0.05, and τ^* is the Shields stress, defined as follows:

$$\tau^* = \frac{C_f U_f^2}{R g D_s} \quad (41)$$

In most sand-bed rivers near a delta the flow is subcritical in the Froude sense, so that Eqs. (36) and (37) reduce to the standard backwater formulation. However, during the course of both experiments described in the companion paper (Kostic and Parker, 2003), the flow was either supercritical or near-supercritical, with the Froude number slightly below unity. In such a case Eq. (37) can be approximated in terms of quasi-uniform normal flow, so reducing with the aid of the closure relation (39) to

$$C_f U_f^2 = -g h_f \frac{\partial \eta_f}{\partial \xi} \quad (42)$$

5.2 Non-dimensionalization

The Eqs. (36)–(38) and (40)–(42) are placed in dimensionless form according to the following algorithm:

$$\begin{aligned} \hat{\xi} &= \frac{\xi}{h_0}, & \hat{h}_f &= \frac{h_f}{h_0}, & \hat{\eta}_f &= \frac{\eta_f}{h_0}, \\ \hat{U}_f &= \frac{U_f}{U_0}, & \hat{q}_w &= \frac{q_w}{h_0 U_0}, & \hat{t} &= \frac{t}{h_0/U_0} \end{aligned} \quad (43a-f)$$

The governing dimensionless parameters for the fluvial model are: river water discharge per unit width q_w , friction coefficient C_f , sand diameter D_S , sand submerged specific gravity R_S , turbidity current depth h_0 and turbidity current velocity U_0 immediately after plunge point, sand porosity λ_S and initial slope S_{f0} of the fluvial bed, here taken to be constant for simplicity.

5.3 Front-fixing modeling

As can be seen in Figure 3, the delta progrades slowly in time. Here both the top and the base of the foreset can migrate in time. To allow for consistency with the turbidity current model, the moving outflow boundary of the fluvial domain is fixed by means of a suitably chosen new coordinate system. A Landau transformation is used to map the spatial domain of the fluvial problem to the finite interval $\zeta^* \in [0, 1]$, with the position of the fluvial channel origin at $\zeta^* = 0$ and the top of foreset at $\zeta^* = 1$:

$$\begin{cases} \zeta^* = \frac{\xi}{f(t)}, & 0 \leq \zeta^* \leq 1 \\ \tau = t \end{cases} \quad (44)$$

where $\xi = f$ denotes the dimensionless position of the fluvial outflow boundary (top of the foreset deposit). The derivatives then transform as

$$\frac{\partial}{\partial t} = \frac{\partial}{\partial \tau} - \frac{\xi^*}{f} \dot{f} \frac{\partial}{\partial \zeta^*} \quad \frac{\partial}{\partial \xi} = \frac{1}{f} \frac{\partial}{\partial \zeta^*} \quad (45a,b)$$

where $\dot{f} = df/dt$ is dimensionless velocity of the top of the foreset. Using Eq. (45a,b) to reduce Eqs. (36)–(38) and dropping the hats for simplicity, the dimensionless equations for the fluvial zone become:

$$U_f h_f = q_w \quad (46)$$

$$\frac{\partial h_f}{\partial \zeta^*} = \frac{-(\partial \eta_f / \partial \zeta^*) - f C_f Fr^2}{1 - Fr^2}, \quad Fr^2 = \frac{U_0^2 U_f^2}{g h_0 h_f} \quad (47a,b)$$

$$\frac{\partial \eta_f}{\partial \tau} = \zeta^* \dot{f} \frac{\partial \eta_f}{f \partial \zeta^*} - \frac{1}{f(1 - \lambda_S)} \frac{\partial q_S}{\partial \zeta^*} \quad (48)$$

Here Fr denotes the standard Froude number of open-channel flow rather than the densimetric Froude number relevant to turbid underflows.

For near-critical or supercritical flow Eq. (42) can be approximated to the form for quasi-uniform normal flow:

$$C_f U_f^2 = -\frac{g}{f} \frac{h_0}{U_0^2} h_f \frac{\partial \eta_f}{\partial \zeta^*} \quad (49)$$

5.4 Initial and boundary conditions

At time $t = 0$, the elevation of topset bed for every grid point within the fluvial domain can be determined from the specified initial slope S_{f0} of the fluvial bed.

If Eqs. (40) and (41) are substituted into the Exner Eq. (38), the resulting equation becomes parabolic. The coordinate system transformation of Eq. (44) introduces additional advective transport as a result of grid stretching. Therefore, both Eqs. (47a) and (48) for near-critical and supercritical flow, as well as Eqs. (48) and (49), for subcritical flow require three boundary conditions: one for the fluvial inflow boundary and two for the fluvial outflow boundary. In the above model the boundary conditions are specified as follows:

$$h_f|_{\zeta^*=1} = Z_l - \eta_f|_{\zeta^*=1} - d \Delta h|_{\zeta^*=1} \quad (50)$$

Here Z_l denotes the water surface elevation of the lake or reservoir, which is taken to be constant in time in the present analysis. In addition, d is a coefficient defined such that $d = 0$ for subcritical river flow into a reservoir or lake (the usual case in the field) and $d = 1$ for supercritical flow into a reservoir or lake. Finally, $\Delta h|_{\zeta^*=1}$ denotes the height of the hydraulic jump formed when supercritical flow impinges upon an infinite body of standing water, given as:

$$\Delta h = \frac{h_f|_{\zeta^*=1}}{2} \left(-3 + \sqrt{1 + 8Fr^2|_{\zeta^*=1}} \right) \quad (51)$$

One of the two flux boundary conditions is given by:

$$q_S|_{\zeta^*=0} = q_{S0} \quad (52)$$

where q_{S0} is the volume sand feed rate per unit width. The second boundary condition describes the relation between the sand delivered to the top of the foreset and the rate of progradation of the foreset. This relation is given by the shock condition (4), which translates to the following dimensionless form:

$$q_S|_{\zeta^*=1} = (1 - \lambda_S) \dot{f} (\eta_f|_{\zeta^*=1} - \eta|_{x^*=0}) \quad (53)$$

where $\eta|_{x^*=0}$ denotes the dimensionless elevation of the toe of the foreset deposit. That is, a sediment delivery $q_S|_{\zeta^*=1}$ to the top of the foreset progrades it at a speed \dot{f} by depositing sediment on it from the top at $\eta_f|_{\zeta^*=1}$ to the toe at $\eta|_{x^*=0}$. In addition to the above boundary conditions the water discharge per unit width q_w must be prescribed and the continuity condition (2) must be imposed.

5.5 Numerical scheme

For subcritical flow Eq. (47a,b) is reduced with Eq. (46) and solved with a Runge–Kutta scheme which is second-order accurate in space. The integration proceeds from the top of the foreset upstream. The morphodynamic part of the model, i.e. given by Eq. (48), is handled by the explicit QUICKEST method described in detail in section 4.5.4.

In the case of supercritical flow the numerical procedure is somewhat more complicated because the boundary condition (50) reduces to a nonlinear equation for bed slope at the top of the foreset. The Exner Eq. (48) is solved by the explicit QUICKEST

method for all computational points except the one farthest downstream, where the slope is determined by a Newton–Raphson iterative procedure. Once slopes are computed at all grid points, the flow field is calculated from Eqs. (46) and (49).

6 Linking of submodels

The fluvial model is linked to the turbidity current model through the continuity condition (2) and the shock condition (53). The progradation rate \dot{f} of the top of the foreset is computed from the fluvial model and Eq. (53). First-order extrapolation on the bottomset bed is then used to determine where the bottomset profile intersects the foreset profile, so satisfying (2) and determining the progradation rate \dot{l} of the toe of the foreset.

The fluvial foreset and turbidity current bottomset communicate morphodynamically with each other through Eqs. (2) and (53). That is, sand delivered to the foreset by the river progrades over the bottomset, so pushing downstream the upstream end of the turbidity current zone. Mud deposited from the turbidity current raises the elevation of the bottomset deposit, so increasing the rate of progradation of the fluvial zone.

7 Sample model application at field scale

A test of the above model against experimental data is provided in the companion paper, Kostic and Parker (2003). It is useful, however, to examine the results of some simulations at field scale in advance. The simulations below are loosely based on the Nemađji River where it flows into Lake Superior at Superior Harbor, Wisconsin. The sediment supply rates have, however, been increased greatly for illustrative purposes. These results were first presented in Kostic and Parker (2000).

In the simulations shown below the water discharge per unit width, as well as volumetric feed rates per unit width of both sand and mud are kept constant over a six-year period. These values should be considered to be typical of a flood flow. If, for example, flood flows occur on the average for three weeks per year, six years of simulated time corresponds to 104.4 years of actual time. This compression of time must be taken into account in interpreting the results.

Initially, the top of the foreset deposit is placed 100 m above its base. The following parameters are the same for all scenarios: bed friction factor $c_D = 0.001$, mud porosity $\lambda = 0.5$, initial slope of the bottomset deposit $S_0 = 0.01$, avalanche angle of the foreset deposit $S_a = 5^\circ$, sand diameter $D_S = 0.5$ mm, sediment submerged specific gravity $R = R_S = 1.65$, sand porosity $\lambda_S = 0.4$, initial slope of the topset deposit $S_{f0} = 0.0001$, water discharge per unit width $q_w = 6$ m²/s and lake water surface elevation $Z_l = 110$ m. The parameters that are varied are: volume sand feed rate per unit width q_{S0} , mud diameter D_M (and thus mud fall velocity v_M) and feed ratio κ defined as follows

$$\kappa = \frac{q_{M0}}{q_{S0} + q_{M0}} \quad (54)$$

where q_{M0} is the mud feed rate per unit width at the upstream end of the fluvial reach (which remains constant over that reach).

The first example, shown in Figures 4 and 5, illustrates the influence of sand feed rate ($q_{S0} = 0.002$ m²/s and $q_{S0} = 0.004$ m²/s) on delta progradation. The input parameters are: $q_{M0} = 0.04$ m²/s and $D_M = 7$ μ m. It can be seen that for the same flow rate, the higher sand feed rate leads to a steeper equilibrium topset slope and more rapid foreset progradation. In this case the small size of the mud results in only a very thin bottomset deposit.

The second example, shown in Figures 6, 7 and 8, illustrates the effect of sediment feed ratio, i.e. fraction of feed that is mud ($\kappa = 0.5$, $\kappa = 0.9$ and $\kappa = 0.95$) on the interaction among the three parts of the deltaic deposit. The input parameters are: $q_{S0} = 0.002$ m²/s and $D_M = 20$ μ m. As expected, a higher fraction of feed that is mud results in a thicker bottomset deposit near the toe of the foreset deposit. Note in the above figures that as the muddy bottomset aggrades it reduces the height of the delta face and causes the sandy foreset to prograde out more rapidly. The sandy foreset in turn buries the bottomset deposit as it progrades over it. The interaction between the sand and mud regions is thus nicely illustrated in these figures, which are quite similar to Figure 3b for the case of the Lake Mead delta.

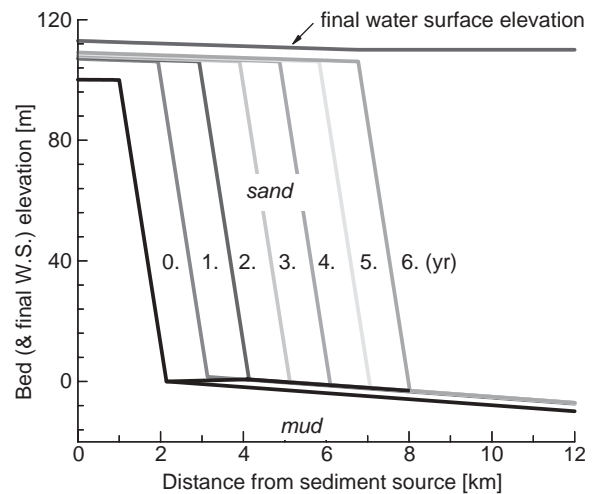


Figure 4 Deltaic progradation for the sand feed rate $q_{S0} = 0.002$ m²/s.

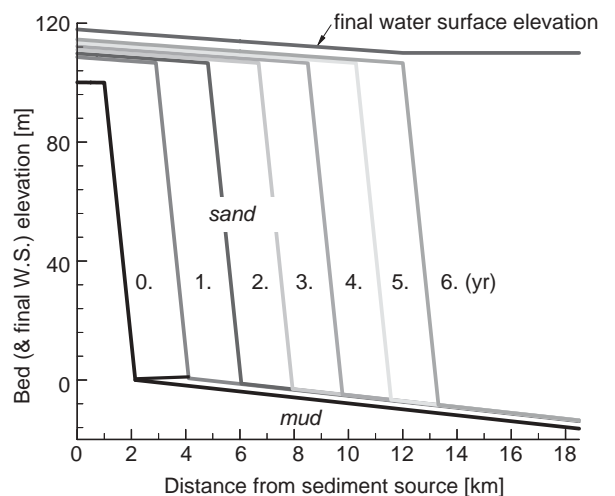


Figure 5 Deltaic progradation for the sand feed rate $q_{S0} = 0.004$ m²/s.

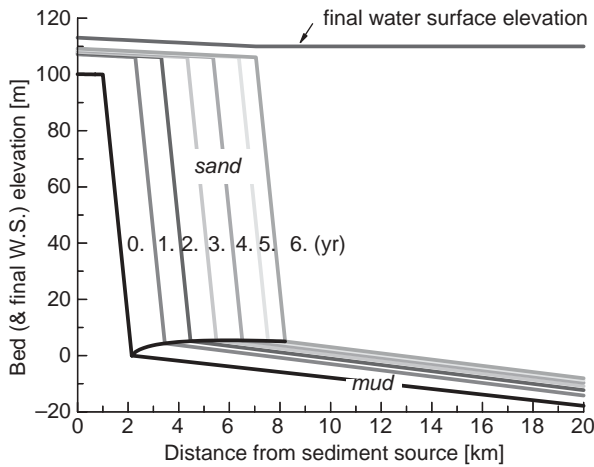


Figure 6 Interaction between the Nemadji River delta and Lake Superior bed with mud as 50% of the sediment feed.

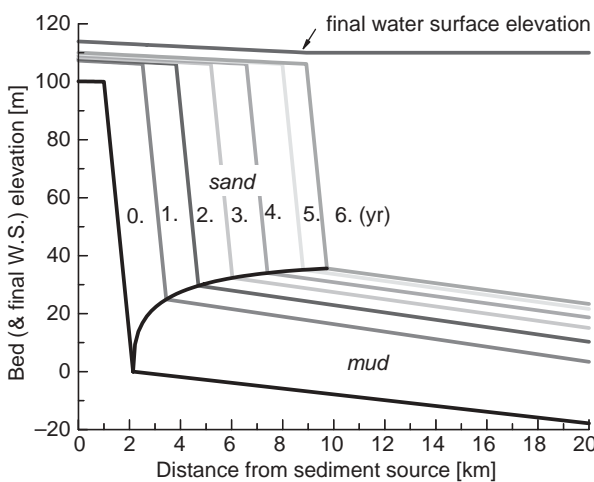


Figure 7 Interaction between the Nemadji River delta and Lake Superior bed with mud as 90% of the sediment feed.

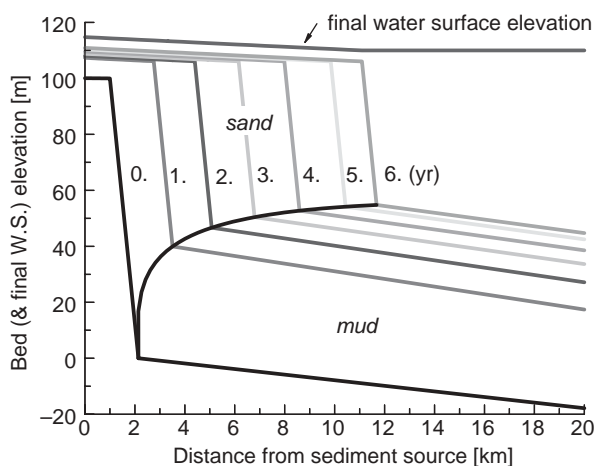


Figure 8 Interaction between the Nemadji River delta and Lake Superior bed with mud as 95% of the sediment feed.

8 Conclusions

The numerical model presented here is the first interactive, physically-based moving boundary model of deltaic sedimentation in lakes and reservoirs. The model dynamically links the fluid mechanics of bottom turbid flows with fluvial dynamics.

As a result, the model is capable of capturing the essence of the topset, foreset and bottomset deposition in lakes and reservoirs, and reproducing for the first time the evolution of the sand–mud interface in deltas.

The modeling of turbidity currents originating from deltas is numerically intriguing since both current boundaries move in time and the governing equations are of the hyperbolic type, admitting shocks and discontinuities. The explicit ULTIMATE QUICKEST method, which is third order in both time and space, provides a robust, mass-conservative formulation that is capable of dealing with complex boundary conditions. The fluvial model is numerically simpler, but still involves one moving boundary. The sediment part of the fluvial model is handled by the explicit QUICKEST method, while the hydrodynamic part is solved with a second-order Runge–Kutta scheme in the case of subcritical flow. For supercritical flow the Exner Equation of sediment continuity is solved by means of the explicit QUICKEST method for all computational points except the one farthest downstream, where the slope is determined by a Newton–Raphson iterative procedure. The two models are linked via numerical inflow boundary condition for the turbidity current domain and physical outflow boundary conditions for the fluvial domain. The computational efficiency of the model is significantly improved by the introduction of time stretching accompanying grid stretching.

When applied to several cases at field scale the model yields interacting topset, foreset and bottomsets that show a structure quite similar to that observed in the delta of the Colorado River on Lake Mead.

The model is validated and applied to various cases in the companion paper, Kostic and Parker (2003). It represents a first step toward a specific field tool for evaluating delta progradation in lakes and reservoirs, as well as reservoir sedimentation. A crucial future step toward this goal is generalization of the model so as to include the transverse flaring outward toward standing water that is characteristic of field deltas.

This work is the result of research sponsored by the Minnesota Sea Grant and the Office of Naval Research STRATAFORM program. The Minnesota Sea Grant College Program is supported by the NOAA Office of Sea Grant, United States Department of Commerce, under grant no. NOAA-NA86-RG0033. The U.S. Government is authorized to reproduce and distribute reprints for government purposes, not withstanding any copyright notation that may appear hereon. This paper is journal reprint no. JR488 of the Minnesota Sea Grant College Program.

Appendix: Derivation of Eq. (4)

Equation (4) describes integral sediment conservation on the foreset. A complete derivation is given below using dimensioned parameters. It is based on the work of Swenson *et al.* (2000), but is here extended considerably beyond the derivation given there.

Consider the foreset illustrated in Figure 1b. Let x denotes distance measured from the sediment feed point and t denote time. The distance from the sediment feed point to the topset–foreset break is f and the corresponding distance to the

foreset–bottomset break is l . At any time the profile of elevation across the delta is given as $\eta(x, t)$. Water surface elevation is given as $Z_l(x, t)$. All the sand is deposited in the topset and foreset, and all the mud is deposited in the bottomset. The foreset slope is $S_a(t)$, where the variation in time may be due to the effect of turbidity currents running over and destabilizing the slope (Kostic *et al.*, 2002). The depth of the river flow at the topset–foreset break is h_f .

The Exner equation of sediment continuity for sand (i.e. topset and foreset) is given by Eq. (3), i.e.

$$(1 - \lambda_s) \frac{\partial \eta}{\partial t} = - \frac{\partial q_s}{\partial x} \quad (\text{A1})$$

Let η_T and η_B denote the bed elevations at the top and bottom of the foreset, respectively. Thus on the foreset

$$\eta = \eta_T - S_a(x - f) \quad (\text{A2})$$

where

$$\eta_T = \eta[f(t), t] \quad (\text{A3})$$

To describe the evolution of the foreset, Eq. (A1) is rearranged and integrate from f to l under the assumption that the sand transport rate precisely vanishes at the toe of the foreset;

$$\int_f^l \frac{\partial q_s}{\partial x} dx = 0 - q_s|_{x=f} = -(1 - \lambda_s) \int_f^l \frac{\partial \eta}{\partial t} dx \quad (\text{A4})$$

where $q_s|_{x=f}$ denotes the value of q_s at the topset–foreset break. Now taking the derivative of (A2) with respect to time

$$\frac{\partial \eta}{\partial t} = \frac{\partial}{\partial t} \eta[f(t), t] + S_a \dot{f} - \dot{S}_a(x - f) \quad (\text{A5})$$

where the dot denotes a derivative with respect to time. In addition,

$$\frac{\partial}{\partial t} \eta[f(t), t] = \frac{\partial \eta}{\partial t} \Big|_f + \frac{\partial \eta}{\partial x} \Big|_f \dot{f} = \frac{\partial \eta}{\partial t} \Big|_f - S_{fT} \dot{f} \quad (\text{A6})$$

where S_{fT} denotes the slope of the topset at the topset–foreset break.

Between (A4), (A5) and (A6) it is found that

$$q_s|_f = (1 - \lambda_s) \left\{ (l - f) \left[(S_a - S_{fT}) \dot{f} + \frac{\partial \eta}{\partial t} \Big|_f \right] - \frac{1}{2} (l - f)^2 \dot{S}_a \right\} \quad (\text{A7})$$

At the topset–foreset break, however,

$$\frac{\partial \eta}{\partial t} \Big|_f = \frac{\partial}{\partial t} (Z_l - h) \Big|_f = \dot{Z}_l - \frac{\partial h}{\partial t} \Big|_f \quad (\text{A8})$$

where Z_l denotes lake (reservoir) elevation and h denotes river flow depth. In addition, Eq. (2) states that

$$\eta_T - \eta_B = S_a(l - f) \quad (\text{A9})$$

Thus (A7) reduces with the aid of (A8) and (A9) to the final form

$$q_s|_f = (1 - \lambda_s) \left\{ (\eta_T - \eta_B) \left[\left(1 - \frac{S_{fT}}{S_a} \right) \dot{f} + \frac{1}{S_a} \left(\dot{Z}_l - \frac{\partial h}{\partial t} \Big|_f \right) \right] - \frac{1}{2} \frac{(\eta_T - \eta_B)^2}{S_a^2} \dot{S}_a \right\} \quad (\text{A10})$$

Equation (4) is recovered under the conditions $\dot{Z}_l = 0$ (constant water surface elevation) and $\dot{S}_a = 0$ (foreset slope that is invariant in time), and the approximations $S_{fT}/S_a \ll 1$ (topset slope is much less than foreset slope) and $(\partial h/\partial t)|_f \ll S_a \dot{f}$ (nearly invariant depth at the river mouth).

Equation (4) thus represents the simplest implementation of a condition that also allows varying lake or reservoir elevation and time-varying foreset slope. The latter case is of interest in that Kostic *et al.* (2002) have illustrated that a turbidity current passing over a foreset can reduce its slope well below the angle of repose, the amount of reduction increasing with the bottom shear stress applied by the turbidity current.

Notation

- c_b = near-bed volumetric concentration of mud
- c_D = bottomset friction coefficient
- C_f = topset friction factor ($=C_z^{-2}$), where C_z is a dimensionless Chezy resistance coeff.
- c_o, c, c_{\pm} = characteristic velocities of the turbid flow
- C = turbidity current depth-averaged volumetric concentration
- C_r = volumetric concentration of mud in the river just before plunging
- d = coefficient that depends on the river flow regime
- D_S, D_M = median diameters of sand and mud respectively
- e_w = water entrainment coefficient
- Fr = Froude number of open-channel flow
- Fr_p = densimetric Froude number associated with plunging
- f = position of the foreset top
- \dot{f} = velocity of the top of the foreset
- g = acceleration due to gravity
- h = turbidity current thickness
- h_f = depth of the fluvial flow
- h_0, U_0, C_0, θ_0 = values of h, U, C and θ_d immediately after the plunge point
- l = position of the foreset toe
- \dot{l} = velocity of the toe of the foreset
- q_a = lake or reservoir flowrate at the river mouth
- q, ϕ, ψ = conservative variables defined such that $q = Uh, \phi = Ch$, and $\psi = \theta_d h$
- q_o = river water discharge per unit width just before plunging ($=q_w$ in the present analysis)
- q_{S0}, q_{M0} = volume discharge per unit width of sand and mud respectively
- q_s = transport rate of sand
- q_w = river flowrate per unit width

R, R_S = submerged specific gravity of mud and sand respectively
 Ri = bulk Richardson number
 Ri_r = river Richardson number
 Ri_0 = Richardson number immediately after the plunge point
 R_p = particle Reynolds number
 r_o = multiplicative constant
 s = position of the front of the turbidity current
 \dot{s} = velocity of the current head
 S_a = avalanche slope
 S_1 = shape coeff. accounting for a nonuniform density distribution over current depth
 S_0, S_{f0} = initial slope of the bottomset and topset bed respectively
 t = time
 u_* = shear velocity
 U = turbidity current depth-averaged velocity
 U_f = river velocity
 v_M = mud fall velocity
 x = bottom-attached streamwise coordinate on lake bed
 x^* = bottom-attached dimensionless streamwise coordinate chosen to be within the finite interval $[0,1]$ on lake bed
 Z_l = water surface elevation of the lake or reservoir
 α = coefficient in the Engelund–Hansen transport relation
 β = local thermal expansion coefficient
 Δ = volume deposition rate of mud per unit bed area per unit time on the bottomset
 Δh = height of the hydraulic jump
 ε = inflow buoyancy parameter
 γ = initial mixing coefficient
 η = elevation of the bottomset as well as foreset bed
 η_f = elevation of the river bed
 η_T = bed elevation at the topset–foreset break
 η_B = bed elevation at the foreset–bottomset break
 φ_{S0} = buoyancy ratio immediately after plunge point
 κ = ratio of mud feed rate to total sediment feed rate (mud + sand)
 λ, λ_S = porosity of mud and sand deposits respectively
 ν = kinematic viscosity of the water
 θ_a = temperature of the lake or reservoir near the bed
 θ_{a0} = lake or reservoir temperature at the river mouth
 θ_r = river temperature just before plunging
 τ = dimensionless time
 τ^* = Shields stress
 θ = turbidity current depth-averaged temperature
 θ_d = turbidity current depth-averaged temperature deviation ($=\theta - \theta_a$)
 ξ = bottom-attached streamwise coordinate in river
 ξ^* = bottom-attached dimensionless streamwise coordinates chosen to be within the finite interval $[0, 1]$ in river

References

1. AKANBI, A.A. and KATOPODES, N.D. (1988). "Model for Flood Propagation on Initially Dry Bed", *J. Hydr. Engrg.*, 114(7), 689–706.
2. AKIYAMA, J. and STEFAN, H. (1984). "Plunging flow into a reservoir: Theory", *J. Hydr. Engrg.*, 110(4), 484–499.
3. AKIYAMA, J. and STEFAN, H. (1987). "Onset of Underflow in Slightly Diverging Channels", *J. Hydr. Engrg.*, 113(7), 825–844.
4. ALTINAKAR, S., GRAF, W.H. and HOPFINGER, E.J. (1989). "Weakly Depositing Turbidity Current on a Small Slope", *J. Hydr. Res.*, 28(1), 55–80.
5. BAINES, P.G. (1999). Downslope Flows into a Stratified Environment – Structure and Detrainment, in "Mixing and Dispersion in Stably Stratified Flows", P.A. Davies (ed.), 1–20.
6. BONNECAZE, R.T., HUPPERT, H.E. and LISTER, J.R. (1993). "Particle-Driven Gravity Currents", *J. Fluid Mech.*, 250, 339–369.
7. BRADFORD, S.F. (1996). Numerical Modeling of Turbidity Current Hydrodynamics and Sedimentation, Ph.D. dissertation, University of Michigan., Ann Arbor.
8. CHIKITA, K. (1989). "A Field Study on Turbidity Currents Initiated from Spring Runoffs", *Water Resources Res.*, 25(2), 257–271.
9. CHOI, S.U. and GARCIA, M. (1995). "Modeling of One-Dimensional Turbidity Currents with a Dissipative – Galerkin Finite Element Method", *J. Hydr. Res.*, 33, 623–647.
10. COOPER, P. and LENSCH, B. (1998). Erosion and Sedimentation in the Nemađji River Basin: Final Report, Nemađji River Basin Project, Natural Resources Conservation Service, U. S. Forest Service, District Conservationist, Ashland, Wisconsin, p. 149.
11. CRANK, J. (1984). Free and moving boundary problems, Clarendon Press, Oxford, p. 425.
12. DIETRICH, E.W. (1982). "Settling Velocity of Natural Particles", *Water Resources Res.*, 18(6), 1626–1982.
13. ENGELUND, F. and HANSEN, E. (1972). A monograph on sediment transport, Technisk Forlag, Copenhagen, Denmark.
14. FAN, J. (1986). "Turbid density currents in reservoirs", *Water International*, 11, 107–116.
15. FARRELL, G.J. and STEFAN, H.G. (1988). "Mathematical Modeling of Plunging Reservoir Flows", *J. Hydr. Res.*, 26(5), 525–537.
16. GARCIA, M. and PARKER, G. (1993). "Experiments on the Entrainment of the Sediment into Suspension by a Dense Bottom Current", *J. Geophys. Res.*, 98, 4793–4807.
17. GRAF, W.H. (1971). Hydraulics of Sediment Transport, McGraw-Hill, New York, p. 513.
18. GROVER, N.C. and HOWARD, C.L. (1937). "The Passage of Turbid Water Through Lake Mead", *Trans. Ame. Soc. Civil Engrs.*, 103, 720–732.

19. IMRAN, J. and PARKER, G. (1998). "A Numerical Model of Channel Inception on Submarine Fans", *J. Geophys. Res.*, 103, 1219–1238.
20. JAIN, S.C. (1981). "Plunging Phenomena in Reservoirs", *Proc. Symposium on Surface Water Impoundments* (ASCE), Minneapolis, MN. U.S.A.
21. KOSTIC, S., PARKER, G. and MARR, J. (2002). "Role of Turbidity Currents in Setting the Foreset Slope of Clinofolds Prograding into Standing Fresh Water", *J. Sedimentary Res.*, 72(3), 353–362.
22. KOSTIC, S. and PARKER, G. (2003). "Progradational Sand-Mud Deltas in Lakes and Reservoirs: Part 2. Experiment and Numerical Simulation", *J. Hydr. Res.*, 41(2), 141–152.
23. KOSTIC, S. and PARKER, G. (2000a). "Modeling of Progradational Sand-Mud Deltas with Plunging Depositional Turbidity Currents", *Proc. 5th International Symposium on Stratified Flows*, University of British Columbia, Vancouver, Canada.
24. KOSTIC, S. and PARKER, G. (2000b). "Front-Fixing Modeling of Turbidity Currents", *Proc. XIII International Conference on Comp. Methods in Water Resources*, Calgary, Canada.
25. LAMBERT, A. (1982). "Turbidity Currents from the Rhine River on the Bottom of Lake Constance", *Wasserwirtschaft*, 72(4), 1–4 (in German).
26. LEONARD, B.P. (1979). "A Stable and Accurate Convection Modeling Procedure Based on Quadratic Upstream Interpolation", *Comp. Methods in Applied Mechanics and Engineering*, 19, 59–98.
27. LEONARD, B.P. (1991). "The ULTIMATE Conservative Difference Scheme Applied to Unsteady One-Dimensional Advection", *Comp. Methods in Applied Mechanics and Engineering*, 88, 17–77.
28. MAHMOOD, K. (1987). Reservoir sedimentation: Impact, extent and mitigation, *Technical paper No. 71*, The World Bank, Washington D.C.
29. MITCHELL, A.R. (1984). in: *Computational Techniques and Applications*, Noye, J. and Fletcher, C.A.J. (eds), 2–14.
30. NORMARK, W.R. and DICKSON, F.H. (1976). "Man-Made Turbidity Currents in Lake Superior", *Sedimentology*, 23, 815–831.
31. PAOLA, C. and PARKER, G. (2000). Criterion for cutoff size of bed material load versus wash load in sand bed streams, *Transactions*, American Geophysical Union, Fall Conference, San Francisco.
32. PARKER, G., FUKUSHIMA, Y. and PANTIN, H.M. (1986). "Self-Accelerating Turbidity Currents", *J. Fluid Mech.*, 171, 145–181.
33. PARKER, G., GARCIA, M., FUKUSHIMA, Y. and YU, W. (1987). "Experiments on Turbidity Currents Over an Erodeable Bed", *J. Hydr. Res.*, 25, 123–147.
34. SAVAGE, S.B. and BRIMBERG, J. (1975). "Analysis of Plunging Phenomena in Water Reservoirs", *J. Hydr. Res.*, 13(2), 187–204.
35. SINGH, B. and SHAH, C.R. (1971). "Plunging Phenomenon of Density Currents in Reservoirs", *La HouilleBlanche*, 26, 59–64.
36. SLOFF, C.J. (1997). *Sedimentation in reservoirs*, Ph.D. Thesis, Technical University of Delft, The Netherlands, p. 269.
37. SWENSON, J.B., VOLLER, V.R., PAOLA, C., PARKER, G. and MARR, J. (2000). "Fluvio-Deltaic Sedimentation: A Generalized Stefan Problem". *Euro. J. Applied Math.*, 11, 433–452.
38. U.S. GEOLOGICAL SURVEY (1986). Suspended Sediment in Minnesota Streams, Report, *U. S. Geological Survey*, St. Paul.
39. TANNEHILL, J.C., ANDERSON, D.A. and PLETCHER, R.H. (1997). *Computational Fluid Mechanics and Heat Transfer*, second edition, Taylor & Francis, Washington D.C., p. 792.
40. VANONI, V.A. (1975). *Sedimentation Engineering*, American Society of Civil Engineers, New York N.Y., p. 745.